applied system innovation

MDPI

Article

The Development and Validation of a High-Resolution Photonic and Wireless System for Knee Gait Cycle Monitoring

Rui Pedro Leitão da Silva Rocha [1], Marcio Luís Munhoz Amorim [2], Melkzedekue Alcântara Moreira [3], Mario Gazziro [4], Marco Roberto Cavallari [5], Luciana Oliveira de Almeida [6], Oswaldo Hideo Ando Junior [7] and João Paulo Pereira do Carmo [2,*]

1 Department of Industrial Electronics, Centro Algoritmi, University of Minho, 4800-058 Guimarães, Portugal; b4094@algoritmi.uminho.pt
2 Group of Metamaterials Microwaves and Optics (GMeta), Department of Electrical Engineering (SEL), University of São Paulo (USP), Av. Trabalhador São-Carlense, Nr. 400, São Carlos 13566-590, Brazil; marciolma@usp.br
3 Department of Mechanical Engineering (SEM), University of São Paulo (USP), Av. Trabalhador São-Carlense, 400, São Carlos 13566-590, Brazil; melkzedekue@usp.br
4 Information Engineering Group, Department of Engineering and Social Sciences (CECS), Federal Univesity of ABC (UFABC), Av. dos Estados, 5001, Santo André 09210-580, Brazil; mario.gazziro@ufabc.edu.br
5 Department of Electronics and Biomedical Engineering (DEEB), School of Electrical and Computer Engineering (FEEC), State University of Campinas (UNICAMP), Av. Albert Einstein 400, Campinas 13083-852, Brazil; mrcavall@unicamp.br
6 Department of Clinical Analysis, Toxicology and Food Sciences, School of Pharmaceutical Sciences of Riberao Preto, University of Sao Paulo, Riberao Preto 14040-903, Brazil; lubio2001@usp.br
7 Research Group on Energy & Energy Sustainability (GPEnSE), Federal Rural University of Pernambuco (UFRPE), Cabo de Santo Agostinho 54518-430, Brazil; oswaldo.ando@ufrpe.br
* Correspondence: jcarmo@sc.usp.br

check for updates

Academic Editors: Cheng-Fu Yang and Igor Korobiichuk

Received: 18 March 2025
Revised: 21 May 2025
Accepted: 10 June 2025
Published: 11 June 2025

Citation: Rocha, R.P.L.d.S.; Amorim, M.L.M.; Moreira, M.A.; Gazziro, M.; Cavallari, M.R.; de Almeida, L.O.; Ando Junior, O.H.; do Carmo, J.P.P. The Development and Validation of a High-Resolution Photonic and Wireless System for Knee Gait Cycle Monitoring. *Appl. Syst. Innov.* **2025**, *8*, 80. https://doi.org/10.3390/asi8030080

Abstract: This paper presents the development and validation of a high-resolution photonic and wireless monitoring system for knee-referenced gait cycle analysis. The proposed system integrates a single optical Fiber Bragg Grating (FBG) sensor with a resonance wavelength of 1547.76 nm and electronic modules with inertial and magnetic sensors, achieving a 10 p.m. wavelength resolution and 1° angular accuracy. The innovative combination of these components enables a direct correlation between wavelength variations and angular measurements without requiring goniometers or motion capture systems. The system's practicality and versatility were demonstrated through tests with seven healthy individuals of varying physical attributes, showcasing consistent performance across different scenarios. The FBG sensor, embedded in a polymeric foil and attached to an elastic knee band, maintained full sensing capabilities while allowing easy placement on the knee. The wireless modules, positioned above and below the knee, accurately measured the angle formed by the femur and tibia during the gait cycle. The experimental prototype validated the system's effectiveness in providing precise and reliable knee kinematics data for clinical and sports-related applications.

Keywords: high-resolution measurement; photonic sensors; fiber Bragg grating; inertial sensors; knee gait cycle monitoring; wireless systems

1. Introduction

Monitoring body kinematics in humans is a growing area of engineering applied to medicine, with universities, high-performance sports centers, and healthcare institutions developing methods to accurately measure and evaluate human body movement for

various purposes [1,2]. The primary objectives for monitoring human body kinematics are to improve athletic performance [3–5] in competitions and to evaluate the efficacy of prescribed therapies and rehabilitation based on information provided by measuring limb movements [6–10]. These efforts have gained traction as musculoskeletal disorders and mobility impairments have become leading causes of disability, making continuous and accurate movement monitoring essential in modern healthcare.

Several monitoring systems have been developed, including electronic systems using wearable wireless sensor networks [11,12], motion capture techniques [13,14], and advanced software algorithms for signal processing and motion classification [15,16]. These systems, while effective, often present limitations in terms of cost, operational complexity, or the requirement for controlled environments, such as motion capture labs. For instance, optical tracking systems, though highly accurate, rely heavily on camera infrastructure and suffer from occlusion issues and limited portability [17,18]. Wearable inertial measurement units (IMUs) offer a more mobile alternative but are often challenged by cumulative drift and magnetic interference, especially in real-world, unsupervised conditions [19–23].

Other applications for limb posture monitoring include assessing certain neurological and orthopedic diseases [19–23], monitoring human biomechanical parameters during rehabilitation [24], and analyzing joint kinematics for fall risk prediction and movement optimization in elderly and athletic populations. In this context, the integration of Fiber Bragg Grating (FBG) sensors into wearable systems has gained notable attention due to their lightweight, electromagnetic immunity, and high strain sensitivity [25]. Several recent studies have explored the use of FBGs for motion monitoring, including systems embedded into insoles, socks, or braces to capture localized mechanical strain related to gait dynamics [17,18].

In a previous study, a gait monitoring system based on optical fiber, complemented by a motion capture system, was proposed. However, this system differs from the solution presented in this paper in several aspects, including the use of a plastic optical fiber (POF), a required calibration procedure, and measurements based on the transmitted optical power when the POF is bent [26]. In contrast, the system presented here uses a silica-based Fiber Bragg Grating, which offers improved spectral resolution and stability for dynamic sensing applications. Additionally, the integration of photonic and inertial modalities allows for cross-validation and redundancy, enhancing system robustness.

Inertial sensors, such as accelerometers and gyroscopes, have been extensively used to monitor human kinematics during the gait process by measuring the acceleration and orientation of specific segments of the arms and legs [27–29]. However, their accuracy can be affected by environmental noise, magnetic field disturbances, or improper sensor placement. To overcome these limitations, hybrid systems combining inertial and photonic sensing have been explored, leveraging the strengths of both modalities. For example, Presti et al. (2020) demonstrated a wearable system for knee monitoring based on FBGs, highlighting improved angular detection when combined with IMUs [25]. Zhao et al. (2022) further emphasized the utility of such hybrid systems in the early detection of neurodegenerative gait anomalies, illustrating their potential for both clinical diagnosis and sports performance tracking [30].

The accurate measurement and characterization of limb kinematics are crucial in diagnosing and treating physical and mental disorders resulting from trauma, stroke, or disease [31]. Developing reliable and precise methods to assess limb movement is essential for both clinical and research purposes. Accurate kinematic data provide valuable insights into the pathophysiology of disorders and support clinicians in determining the most effective treatments and therapies for their patients. Therefore, advanced techniques and technologies for kinematic analysis should be prioritized in the medical field. This demand

has led to the increasing adoption of smart, wearable devices that are easy to use, minimally invasive, and capable of operating in real-world environments without dependence on external infrastructure.

The main contribution of this paper is the joint utilization of two wearable/attachable photonic and wireless systems with high resolution for characterizing the knee gait cycle. This approach allows for the construction of a chart representing wavelength variation versus angular variation, bridging the gap between photonic strain sensing and biomechanical motion estimation. The designed and fabricated system offers numerous advantages in biomedical fields, particularly in physical therapy and athletic assessment applications, due to its high resolution, wireless transmission capability, and ease of application to the targeted body region. It permits the precise measurement, recording, and evaluation of distinct mechanical parameters of limb motion. Primary end-user applications include patients with conditions affecting bones, muscles, and joints, as well as athletes. The system's capability to provide objective measurements of limb motion parameters supports effective diagnosis, therapy, and rehabilitation interventions.

Despite advances, there is still a gap in the literature regarding the development of solutions that combine high-resolution photonic and wireless electronic sensors to characterize the knee gait cycle without using complex motion capture systems. While existing research has explored FBG systems and IMU platforms independently, few studies have successfully integrated them into a unified, low-complexity wearable solution validated on multiple subjects. This study aims to develop and validate an innovative system to measure knee-referenced gait cycles using photonic and wireless systems, providing a practical and high-resolution solution for medical and sports applications. The justification for this work lies in the need for more accessible, accurate, and user-friendly monitoring systems for diagnosing and tracking patients in physical therapy and athletic evaluations.

The main highlights of this study include (i) an innovative combination of photonic sensors and wireless electronic modules for gait monitoring; (ii) a high resolution with sensors of 10 p.m. and an angular accuracy of 1°; (iii) biomedical applications in physical therapy, rehabilitation, and athletic assessments; and (iv) system testing on individuals with different physical attributes, demonstrating consistency and versatility. The structure of this article is organized as follows: Section 2—Methods: Detailed description of the proposed system, including photonic and wireless components. Section 3—Measurements: Presentation of data obtained from experimental tests with seven volunteers. Section 4—Results and Discussion: Critical analysis of the results and a comparison with previous studies. Section 5—Conclusions: Summary of the main contributions and suggestions for future studies.

2. Methods

This section presents the methodology applied in this study, including the design, development, and implementation of the proposed system for knee gait cycle monitoring. The methodology is divided into specific components, such as the photonic and wireless systems, experimental procedures, and data analysis methods. Each subsection provides a detailed explanation of the approaches and technologies used to ensure the accuracy, reliability, and versatility of the proposed system.

2.1. Photonic Component

The system proposed in this paper is based on Fiber Bragg Grating (FBG) technology, which comprises a sensing module and a monitoring module. Figure 1 displays the photonic component of the system, which incorporates a light source and an interrogation system used for monitoring the received light. The FBG is embedded in a PVC foil within

the knee band, which is visible in the photograph. The hardware and software components are used for interrogating and analyzing the light signals, which are then displayed on a computer screen. The FBG-based system provides an efficient means of measuring the mechanical parameters of human limb motion, enabling objective and reliable data for applications such as physical therapy and athletic assessments. This light source presents a FWHM (full width at half maximum, e.g., the bandwidth measured at 3 dB) of 60 nm, where a maximum ripple of 0.2 dB was able to produce a broadband light beam in the desired wavelength range. Moreover, this optical source is able to generate optical beams with an output power up to 8 mW.

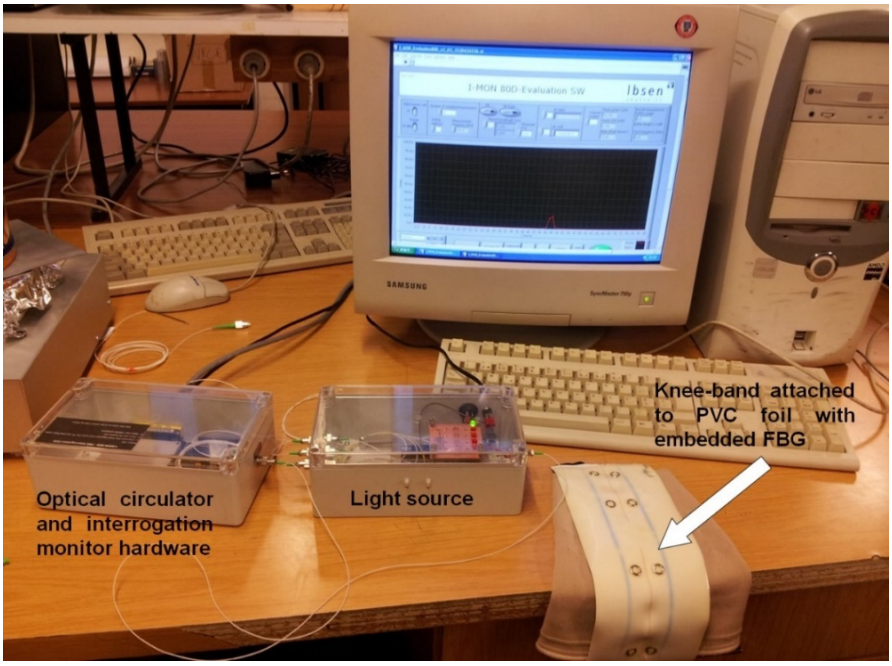

Figure 1. Photonic component's setup, with the knee band already connected. It is composed of a light source, an optical circulator, and an interrogation monitor hardware.

The FBG was inscribed in a hydrogen-loaded standard telecommunication fiber, specifically the Corning SMF-28e+ from Corning Incorporated, headquartered in Corning, New York, NY, USA, using a pulsed excimer laser from Coherent Inc., located in Santa Clara, CA, USA, and the phase mask technique. The resulting grating has a length of 8 mm and a resonance wavelength of 1547.76 nm, corresponding to a core refractive index modulation period in the half-micrometer range.

The interrogation monitor allows real-time spectrum monitoring of FBG sensor interrogation systems and uses two transmission gratings to split spatially the wavelength spectrum as well as a parabolic mirror to focus each component to a specific pixel in the imager. The optically sensitive part of the imager is an Andor iDus InGaAs 1.7 detector (Andor Technology Ltd., Belfast, Northern Ireland, UK), operated with a region of interest (ROI) comprising 80 pixels. This configuration provides an intrinsic spectral resolution of 0.4 nm, distributed over the usable spectral range (e.g., 1529–1561 nm).

The proposed application benefits from the features of the optical detector, including a dynamic range of 30 dB, a maximum wavelength drift of 2 p.m. per 1°, an input optical power range of 10–50 dBm, and a power consumption of 250 mW. In addition, the manufacturer provides a software that allows for the real-time visualization of waveforms during sensor activation. This system has a spectral resolution of 10 p.m., which was measured in terms of −20 dBm input power and a low-loss optical circulator. An optical circulator

was also used for separating the reflected light from the injected spectrum. The optical circulator operates in the 1525–1565 nm range, and it was selected as it allowed all detectable wavelengths to pass. Moreover, the optical device possesses a range of additional attributes, including a typical insertion loss of 0.7 dB (where the power loss remains below 15% of the total), a maximum polarization loss of 0.2 dB (equivalent to a maximum of 5%), a reverse-to-direct input isolation of at least 50 dB (with less than 0.01% of the optical power injected into the reverse input leaking into the direct one), and a maximum optical power capacity of 500 mW.

Because this system has a high resolution, it allows for the addition of several more FBGs in the same fiber since all of them can be individually differentiated from one another even if they have a very close resonance wavelength. What limits the system's resolution is the dynamic range of each sensor so that no peak overlaps the adjacent one. This could be used for expanding the photonic system to measure several joints in a human body using just one fiber and the same setup, as presented in Figure 1. The acquired data can be stored for subsequent analysis and investigation, thereby facilitating temporal comparisons. Furthermore, the developed system was engineered to achieve maneuverability, thereby enabling it to be compatible with a wide range of body kinematic movements. In Figure 2 the block diagram of the FBG's measuring system is represented.

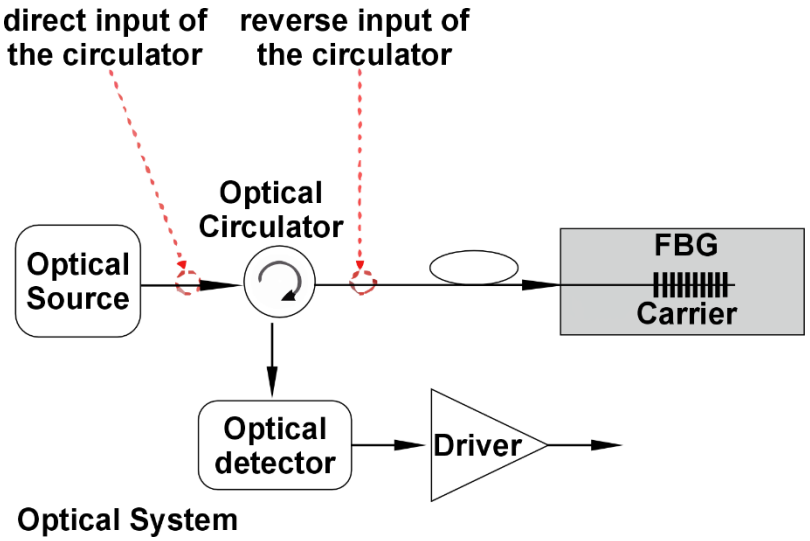

Figure 2. The block diagram of the proposed measuring system for the FBG sensor.

The gait monitoring system, the Fiber Bragg Grating (FBG) sensor, and the wireless inertial modules function as complementary components, each capturing distinct yet correlated aspects of knee joint biomechanics. The FBG sensor measures localized strain on the surface of the knee, providing high-resolution data on deformation caused by flexion and extension during walking. Simultaneously, the wireless modules comprising accelerometers and magnetometers track the angular orientation of the femur and tibia, capturing dynamic joint movement throughout the gait cycle. While these two sensing modalities operate in parallel, they do not require real-time mutual calibration. Instead, during system development, an initial correlation phase is performed where the FBG wavelength shifts are experimentally mapped to the angular displacements recorded by the inertial sensors. This one-time regression mapping allows the strain data from the FBG sensor to be interpreted in terms of joint angles, thereby enabling synchronized and accurate motion analysis. Once calibrated, the sensors can operate independently in practice, provided they are placed consistently. This dual-sensor approach enhances the

system's overall robustness and accuracy by combining high-resolution strain detection with three-dimensional angular tracking.

2.2. Wireless Component

The wireless component is an electronic system composed of two sensor modules and a base station which collects data and relays it to a PC through a serial connection. A sensor module is presented in Figure 3. Each module is composed of two boards. One of them includes a CC2530 microcontroller from Texas Instruments (Dallas, TX, USA), which integrates an IEEE 802.15.4-compliant transceiver operating in the 2.4 GHz frequency band and supports wireless communication protocols such as Zigbee (see Figure 3a). The other board has the sensors (one three-axis accelerometer and one three-axis magnetometer) and a rechargeable battery to power the system (see Figure 3b).

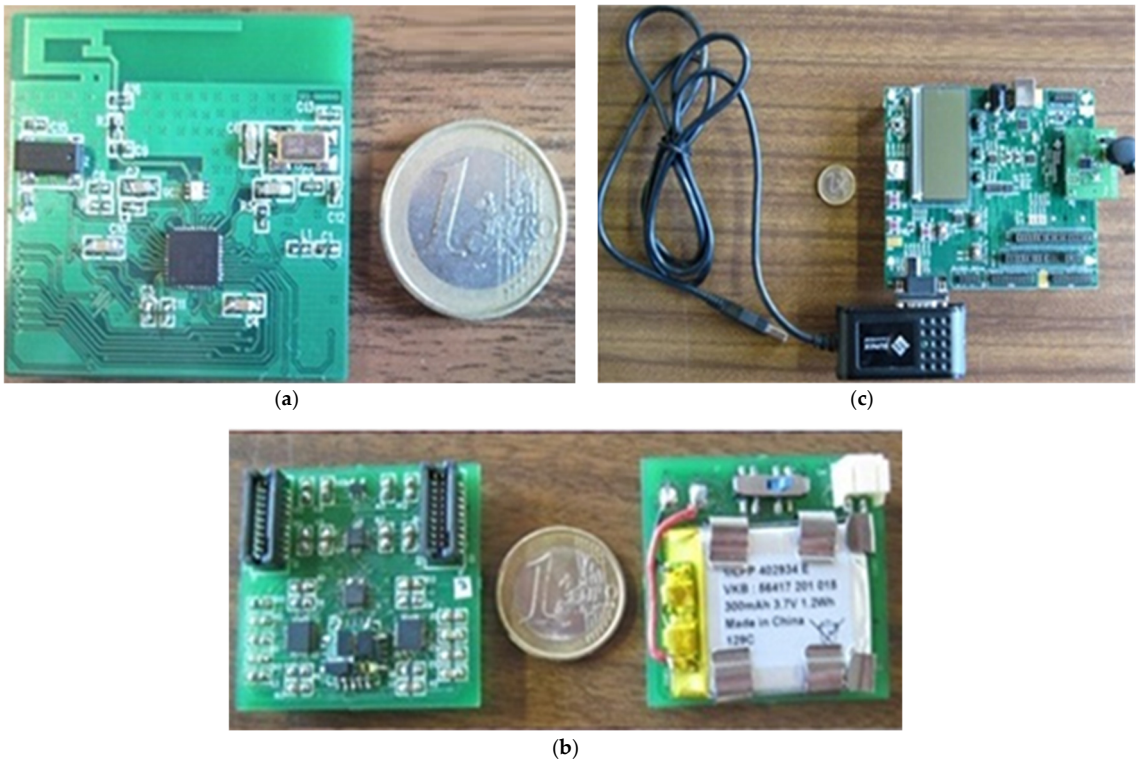

(**a**) (**c**)

(**b**)

Figure 3. Photographs of the modules with the sensors: (**a**) the radio module with the PCB antenna, (**b**) the PCB containing the accelerometer and magnetometer sensors, and (**c**) the base station of the wireless electronic system.

The microcontroller board connects to the sensor board through two 20-pin header connectors. The sensor board incorporates the LIS331DLH accelerometer, a three-axis MEMS sensor manufactured by STMicroelectronics (Milan, Italy). This device offers 12-bit digital output resolution, with a sensitivity of 1 mg, and supports a selectable output data rate ranging from 0.5 Hz to 1 kHz. The magnetometer used is the XEN-1210, a high-precision three-axis Hall-effect magnetic field sensor developed by Sensixs Design (Delfgauw, The Netherlands). It provides nanotesla-level resolution for magnetic field measurements along the X, Y, and Z axes. The data output is 24 bits with a sensitivity of 15 nT, allowing a sample rate of up to 5 kHz. The sensor module collects data from the onboard sensors and transmits it to the base station (Figure 3c) using a customized medium access control (MAC) protocol, known as eLPRT (enhanced Low-Power Real-Time) [32]. This protocol is specifically designed to support low-latency and energy-efficient wireless communication, which is critical for battery-operated systems. Because the modules are

compact, wireless, and battery-powered, they can be unobtrusively placed on various parts of the user's body, enabling unrestricted movement and seamless monitoring.

The base station controls the wireless network performing coordination functions. Such functions include the registering of sensor modules in the network, maintaining synchronization with the help of transmitted periodic beacons, and allocating slots of time for data transmission and retransmission every time an error occurs. The synchronous nature of the implemented MAC layer protocol makes the messages arrive at specific points in time. The hardware generates an interrupt signal to handle the packet every time a message arrives. Then, the MAC header of the message is removed, and the payload of the message is sent using the RS232 serial port to the PC. The block diagram of the electronic component in the proposed system is represented in Figure 4.

The acquisition of data from the accelerometer (LIS331DLH) and magnetometer (XEN1210) is achieved through the SPI bus, and the sensor module utilizes the DMA subsystem to control the USART and radio peripherals. The obtained data is transmitted to the base station via the eLPRT protocol. The wireless sensing modules were attached to the leg with a generic 25 mm white Velcro straps onto the lower thigh (femur) and upper leg (tibia), as shown in Figure 5. Using the foil with the attached FBG as a reference and directly covering the patella, the top sensorial module was strapped on top of the foil (due to the existence of the antenna), and the bottom sensorial module was strapped behind the foil. This type of sensor placement aligns the two electronic modules with the FBG sensor. The base station used for the wireless communication was placed a few meters away in order to reduce data loss during the tests. As demonstrated in Figure 5, the angle calculated for each sensorial module is the lowest angle between the system's z-axis and the module's z-axis when in that position. The volunteers stated that these straps were comfortable to use and did not interfere with their normal walking process.

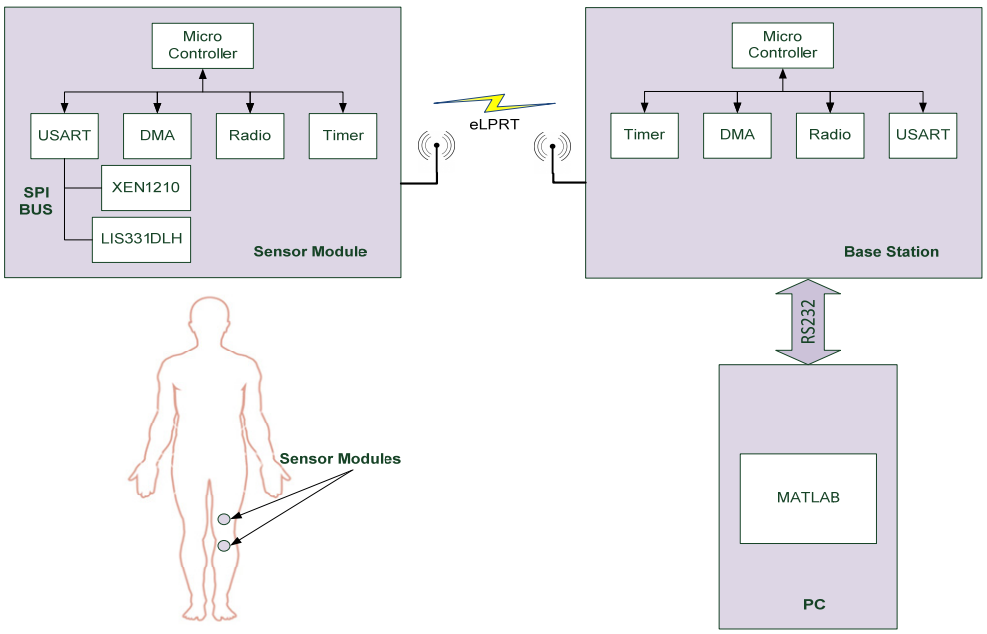

Figure 4. Block diagram of the sensor modules and base station for the electronic component.

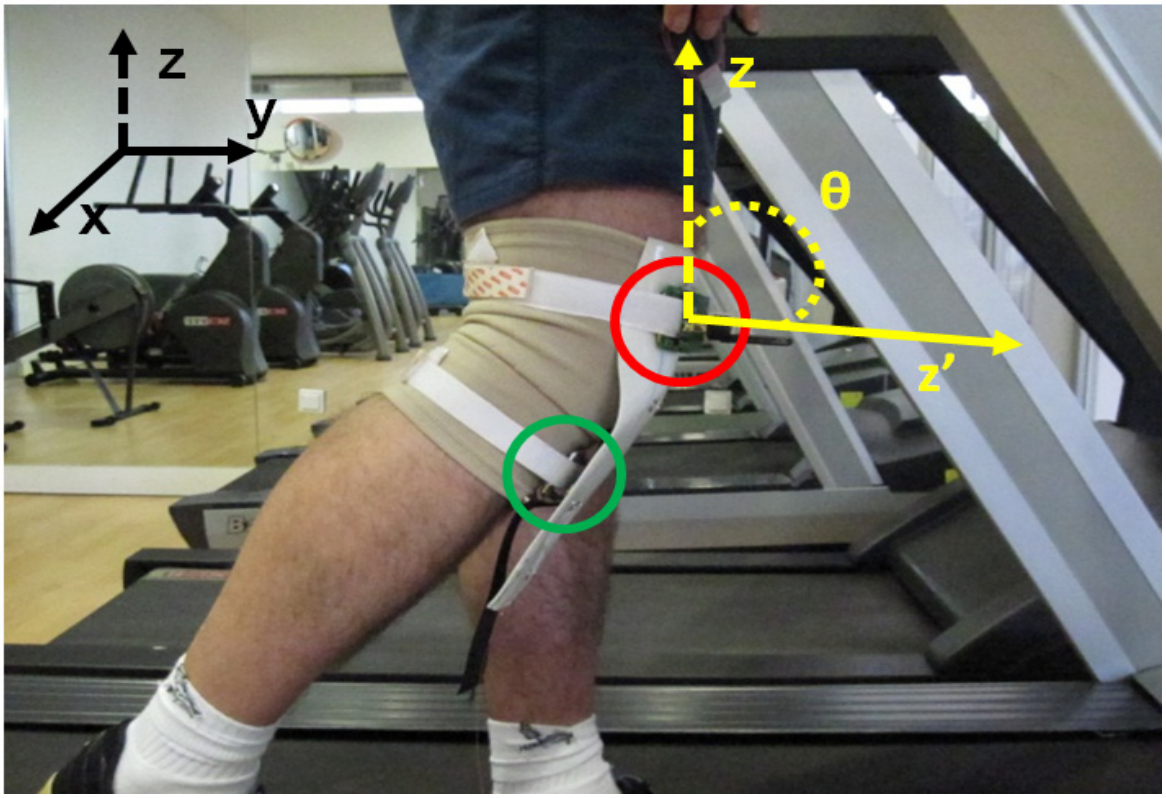

Figure 5. The inertial modules were strapped with Velcro straps onto the lower thigh (marked with a red circle) and upper leg (marked with a green circle), measuring the different angles obtained by these sections of the leg during a full gait cycle. The placement of the inertial modules in relation to the foil with the FBG.

2.3. Design and Implementation Approach

The gait cycle is the summation of two phases of a complete step, namely the stance and swing phases. The stance phase corresponds to the duration during which the foot contacts the ground, while the swing phase corresponds to the time when the foot is lifted off the ground and moves forward in the air, facilitating the advancement of the body. Knee kinematics is represented by two cycles, flexion and extension. The objective is to represent graphically, as a function of the measured wavelength and the measured angle made between the tibia and femur, the full human gait period centered on the knee joint. This is performed by using just one FBG, a single-mode optical fiber, and electronics modules based on two modules, with each containing 3-axis accelerometer and magnetometer sensors that are used to measure their relative angle.

The main objective of this study is to validate the proposed concept by measuring the knee's kinematics. For this purpose, a single FBG sensor and a single fiber are placed at the center of the knee joint, while two electronic modules are positioned above and below the knee to measure the subject's motion. To detect the complete range of knee movement during gait, a highly sensitive sensor is required, which can accurately capture movements from the leg's completely straight position to the maximum knee deflection during gait, including the stance and swing phases. The sensing system is designed as a flexible structure that can be easily attached and removed from the knee using small pressure buttons. Figure 6 illustrates the metallic pressure buttons used to attach the various components of the sensing system, including the elastic knee band and the foil with the embedded FBG. The benefits of using FBG sensors as embedded sensing devices are discussed in detail in reference [33].

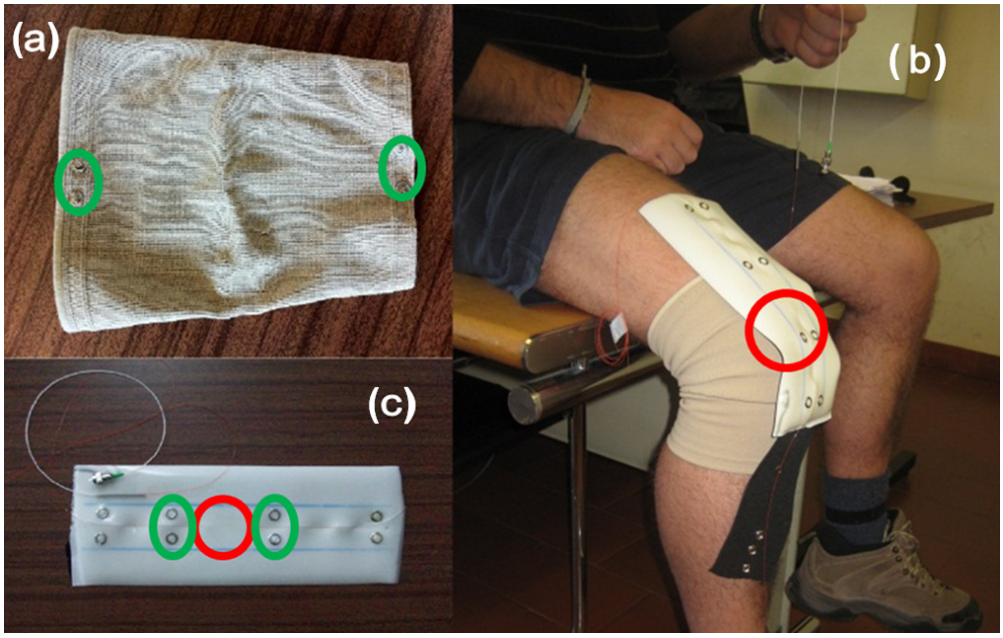

Figure 6. Photographs of the knee band apparatus: Panel (**a**) shows the elastic knee band, with green ellipses marking the position of the pressure buttons. Panel (**b**) shows the sensing component attached to the standard elastic knee band. Panel (**c**) is a close-up of the PVC foil containing the embedded FBG, indicated with a red circle, and the pressure buttons are marked with green ellipses [34].

The elastic knee band utilized in this study is commonly employed as a precautionary measure for individuals with temporary or permanent muscle injuries, allowing for the flexible structure to be used by anyone and in any part of the body. The use of pressure buttons guarantees that the sensing component can accurately measure knee flexion and extension during subject movement. The immunity of optical fibers to electromagnetic interference (EMI), as well as their ability to operate effectively in wet environments or underwater, increases the range of potential applications for this technology.

Temperature variation is a well-known challenge in Fiber Bragg Grating (FBG) sensor systems, as it affects both the grating period and the effective refractive index of the fiber core, leading to wavelength shifts that can be misinterpreted as mechanical strain. In this work, temperature effects were minimized primarily through signal processing, specifically by applying a high-pass finite impulse response (FIR) filter with a 15 Hz cutoff frequency. This filter effectively eliminates low-frequency components, such as slow temperature drifts, while preserving the higher-frequency signals associated with dynamic limb movement. However, in scenarios where quasi-static measurements or variable environmental conditions are involved, more robust compensation strategies may be required. A commonly used method involves the inclusion of a second, mechanically isolated FBG sensor exposed to the same thermal conditions; the differential signal between the two FBGs provides a temperature-compensated strain measurement. Alternatively, FBG packaging with thermally matched or insulating materials can reduce sensitivity to ambient fluctuations by minimizing thermal gradients. For advanced applications, dual-parameter FBG systems employing two gratings with distinct sensitivities enable matrix-based decoupling of temperature and strain signals. Moreover, software-based post-processing using pre-characterized calibration curves can offer additional correction when direct hardware compensation is not feasible. These techniques, when integrated appropriately, ensure that FBG-based systems maintain high accuracy even under varying thermal environments, enhancing their applicability in real-world biomechanical monitoring scenarios.

2.4. Signal Processing of the FBG Sensor

The Fiber Bragg Grating (FBG) is fundamentally characterized by a periodic variation in the refractive index along the fiber axis [34]. In addition to the common benefits associated with optical fiber sensors, FBGs possess an intrinsic self-referencing and multiplexing ability. This structure operates as a reject-band filter, reflecting back the spectral component, λB [nm], that meets the Bragg condition (provided by Equation (1)) while allowing the transmission of the remaining components. The Bragg wavelength can be calculated as [35–37]

$$\Delta\lambda = K\varepsilon X \times \varepsilon \quad (1)$$

The wavelength shift, ΔλB [nm], of an FBG sensor due to a physical disturbance is determined by the grating pitch, Λ, and the effective refractive index of the fiber core, neff. The expression for ΔλB [nm] is given by Equation (2) [38–40]:

$$\frac{\Delta\lambda_B}{\lambda_B} = (1-\rho_e)\Delta\varepsilon + (\alpha+\xi)\Delta T \quad (2)$$

Equation (2) describes the wavelength shift, ΔλB [nm], of a Fiber Bragg Grating (FBG) sensor due to a physical disturbance. The components involved in the equation are ρe, which represents the effective photoelastic constant; Δε, which represents the axial strain; α, which represents the thermal expansion; ξ, which represents the thermal optic coefficient; and ΔT, which represents the temperature shifts. The first term in the equation expresses the strain effect on an optical fiber, which causes a change in the grating spacing and the refractive index due to strain–optic effects. The second term is related to temperature sensing, as changes in temperature cause the FBG to dilate or contract, modifying the grating pitch.

As seen in Equation (2), FBGs are susceptible to temperature fluctuations. The leg movements' frequency measured in this gait analysis method is faster than the temperature variations (both room and body temperatures). Therefore, the temperature variations could be seen as a DC signal being introduced in the AC signal from the readings obtained. Moreover, with the utilization of a high-pass filter, which is presented in Section III B, the temperature effect is negligible.

2.5. Flexible Sensing Structure

To achieve accurate measurement of knee joint movement, it is necessary to increase the dynamic range of the sensor. This can be achieved by selecting a substrate material that conforms well to the actual movement. Therefore, a structure with sufficient area to cover the knee is required to transfer the movements to the embedded sensor. A wide rectangular configuration was chosen to cover both flexion and extension movements, as it provides the necessary contact area to be sensed and allows the light to travel smoothly without any abrupt corners that could hinder communication with the monitoring stage. The main characteristics and advantages of this foil include flexibility, stretchability, and the capability to sustain a good bonding between the optical fiber and the substrate. The host material used is polyvinyl chloride (PVC) with a custom formulation that ensures proper bonding and stimulus transfer [41]. The size and shape of the material can be fully customized during fabrication.

2.6. Angle Measuring Using the Wireless Electronic Component

The accuracy of the wireless electronic system is fundamentally influenced by the noise characteristics of its inertial sensors. To validate the claimed angular measurement error of ±1°, a calibrated digital protractor was used as a reference instrument. The knee joint was manually positioned at known angles, such as 30°, 45°, 60°, and 90°, and the corresponding

readings from the wireless system were recorded in parallel. The comparison between the digital protractor and the inertial module outputs revealed a maximum deviation of less than 1°, confirming the system's angular accuracy under controlled conditions. This result supports the suitability of the wireless module for precise joint angle tracking in clinical gait monitoring applications. The calibration of the sensors is important to minimize offsets. Therefore, the sensors must be calibrated and configured on-site through the base station. A sampling period of 33 milliseconds was used, which is enough to capture the desired knee movement. The sensor node generates a packet with three samples at each superframe, which is configured for 100 milliseconds. The base station uses an RS232 serial port to communicate with the PC. The data is further processed by the PC using Matlab v24.1. The accelerometer and magnetometer readings are converted into angles (e.g., pitch, roll, and yaw) using a pre-compiled algorithm. Due to the inclination of the magnetic pole relative to the earth's surface, the magnetometer readings are previously compensated in order to extract only the horizontal components (X_h,Y_h), so an angle can be produced in the azimuth plane. Furthermore, since any acceleration apart from gravity induces errors in angle measurements, a compensation algorithm is applied to the inertial sensors in order to minimize errors due to accelerations during the motion of the body. When accelerometer calibration takes place, the gravity values are obtained for each axis. These values are used to normalize readings, producing outputs in the range of -1 to 1 (as in 'g' forces) when no external force besides gravity is present. When a measurement is collected, the acceleration vector is normalized, and its module must be equal to 1 (within a certain minimum threshold in the order of 10-3) when gravity is the only force being applied. When the acceleration module is not equal to unity, the measurement contains acceleration besides gravity. Since the magnetic sensor does not depend on the acceleration of the body, it is used to compensate the acceleration measurement when this happens. The values from the previous and current magnetic readings are used to compute the angle and axis of rotation that occurred during two consecutive readings. The axis and angle are then used to rotate the previous gravity vector to the new orientation that is being described in current measurements. This method allows for the separation of the gravity force from other accelerations present in the acceleration measurement by simply subtracting the gravity component from the original acceleration reading. Pitch, roll, and yaw angles are computed using the gravity part of the acceleration vector. The axis and angle of rotation are obtained using Equations (3) and (4):

$$angle = \arccos\left(\left\|\vec{M}_{n-1}\right\| \bullet \left\|\vec{M}_{n}\right\|\right) \tag{3}$$

$$axis = \left\|\vec{M}_{n-1}\right\| \times \left\|\vec{M}_{n}\right\| \tag{4}$$

Equation (3) uses the dot product of the normalized vectors to obtain the smallest angle between the previous and current magnetic vectors. In Equation (4), the cross product between the previous and current normalized magnetic vectors produces the rotation vector, by which the previous gravity vector (the acceleration vector without any force besides gravity) is rotated. The rotation of the previous gravity vector is performed and has been described in [42]. The pitch, roll, and yaw angles are obtained using Equations (5)–(7), respectively.

$$Pitch = \arctan\left(\frac{a_y}{\sqrt{a_z^2 + a_x^2}}\right) \tag{5}$$

$$Roll = \arctan\left(\frac{a_x}{a_z}\right) \tag{6}$$

$$Yaw = \arctan\left(\frac{X_h}{Y_h}\right) \tag{7}$$

These angles are calculated according to the axis represented in Figure 7, which depicts a left-handed coordinate system. The orientation of the sensorial modules in space is thus represented with a forward orientation along the y axis, with pitch defining the rotation on the x-axis, roll on the y-axis, and finally yaw on the z-axis.

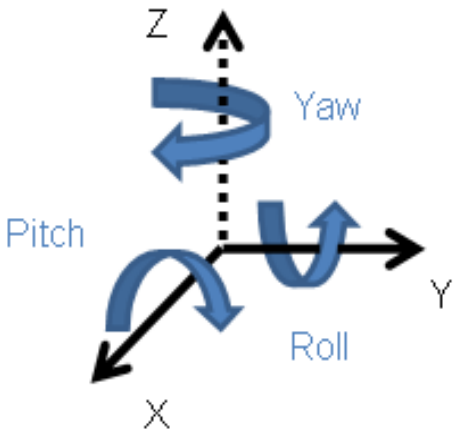

Figure 7. A representation of the system axis and the left-handed coordinate system.

The vector $\vec{v}_i$ in Equation (8) is a representation of the module's orientation after its rotation. Now that the orientation of each module is known, the lower angle between the vector of the module and the z-axis, represented by the vector $\vec{u}$ in Equation (9), is calculated using the inner product space, as seen in Equation (10). The angle θ_i, formed during the gait cycle, is the subtraction of the angle measured by the lower and upper parts of the leg, namely the femur and tibia, respectively. This method is more tolerant regarding the placement of the modules in the user's body, since it accounts for any kind of tilt which influences the axis we want to measure (z-axis), in contrast with, for example, measuring only the roll angle of both modules.

$$\vec{v}_i = [x_i, y_i, z_i] \tag{8}$$

$$\vec{u} = [0, 0, 1] \tag{9}$$

$$\theta_i = \arccos\left(\frac{\vec{v}_i \bullet \vec{u}}{\left|\vec{v}_i\right|\left|\vec{u}\right|}\right) \tag{10}$$

3. Measurements

This section presents the measurements obtained using the proposed photonic and wireless monitoring system for knee-referenced gait cycles. The collected data includes both raw and processed measurements, demonstrating the system's ability to accurately capture knee kinematics under different testing conditions. Additionally, the results highlight the system's consistency, versatility, and potential for clinical and sports-related applications, validating its effectiveness in monitoring and analyzing human gait dynamics.

3.1. Experimental

Seven healthy individuals volunteered to perform the presented tests (four of them being male), and their characteristics and statistical information are summarized in Table 1. The only condition involved in accepting the volunteers was to find subjects with clear physical and age differences to expand the system's flexibility of use and certify the ability

to differentiate the individual gaits, such as between volunteers C and E. The mean and standard deviation values for the height (cm), weight (kg), and age are {170.29; 10.7}, {68.36; 12.26}, and {35.14; 18.84}, respectively.

The knee kinematics is characterized mainly by the flexion and extension movements, and two different kinds of data are provided in this paper. To monitor knee movements, a flexible polymeric foil prototype with an embedded sensor was applied to an elastic knee band. The FBG was positioned on the patella using pressure buttons as bonding elements. Raw data was collected by the FBG with subject A while they walked and ran on a commercially available treadmill found in gymnasiums, validating the consistency and reliability of the system. The dataset is shown in Figure 8.

Table 1. Subjects' physical information and statistical data.

Volunteer	Height (cm)	Weight (kg)	Age (years)
A—Male	177	77	35
B—Female	159	60	17
C—Female	158	55.5	64
D—Female	163	59.5	18
E—Male	185	90	24
F—Male	170	63.5	30
G—Male	180	73	58
Mean	170.29	68.36	35.14
St. Dev.	10.70	12.26	18.84

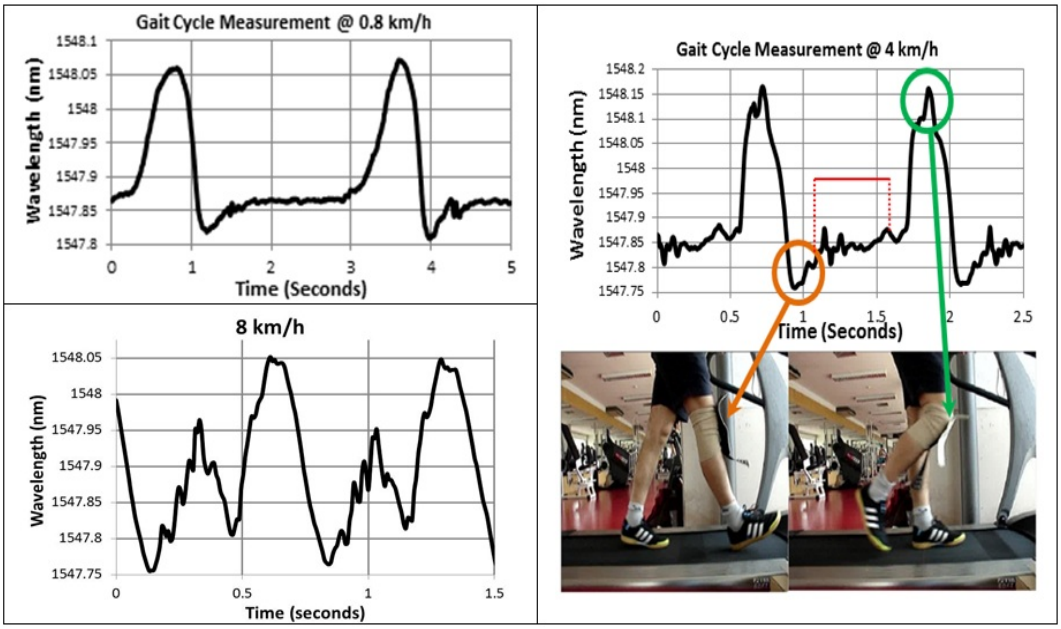

Figure 8. The figure shows the raw, unfiltered data measured by the FBG for two full gait cycles at three different speeds. The swing and stance phases of the gait cycle are indicated by the minimum and maximum deflections of the FBG, respectively, and the time between them. This data validates the consistency and reliability of the system [34].

3.2. FBG Data

Figure 9 shows the measurements of both systems (data already filtered) in all seven subjects. The sessions were performed with the volunteers walking on a treadmill at a constant speed in order to have a common comparison reference. Although the same treadmill speed allows for a meaningful comparison of kinetic parameters between sessions, deviations in normal gait dynamics, such as cadence, stride length, and knee flexion

angle [41,43,44], still occur. The experimental tests were conducted for 10 s, but only two complete gait cycles were considered to enhance the clarity of the unfiltered data. Figure 8 displays the raw waveforms acquired by the FBG sensor for three different walking speeds: 0.8 km/h (0.22 m/s), 4 km/h (1.11 m/s), and 8 km/h (2.22 m/s). The waveform sharpness increases with the increase in walking speed. However, the running movement is characterized by a quicker step, leading to waveform sharpness and slight kinematic variations, particularly when the front foot lands on the ground and propels the body forward. Nevertheless, the results facilitate the identification of various events that occur during the walking and running movements.

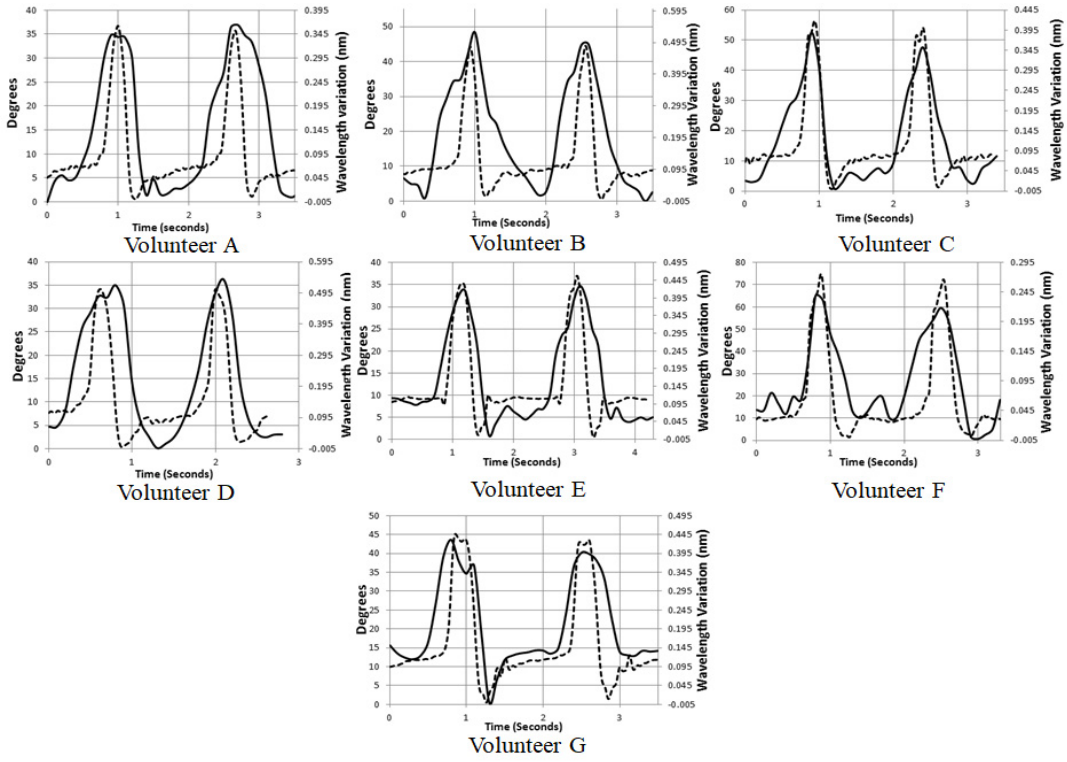

Figure 9. Demonstration of the FBG wavelength shift signals recorded from seven different subjects.

To compare the measured period of the data with different steps in a complete cycle, Figure 8 presents the two extreme values acquired by the system during a full step cycle of 2.5 s at 4 km/h. The minimum deflection is observed when the leg is in the stance phase and the knee joint is flexed, corresponding to a value of 1547.76 nm (resonance wavelength). On the other hand, the maximum deflection is observed when the leg is in the swing phase, corresponding to a value of 1548.16 nm. The period between these two extremes of movement is characterized by low-amplitude variations that follow the knee movement when the leg is in contact with the floor. Notably, during the period between the minimum and maximum values, the leg remains in contact with the floor (stance phase), and the FBG sensor is substantially stretched, with minor variations attributable to the elastic knee band. This relatively constant period is highlighted in red in Figure 8. The right leg begins its movement backward, with the ankle touching the floor first, followed by the base of the foot until it starts moving forward with the tip of the toes (the maximum deflection in the figure represents approximately 80% of the gait period) [42].

The FBG sensor system allows for the detection of various movements, such as flexion and extension, which are associated with a complete step, thereby enabling the comparison of results acquired in various scenarios involving different subjects. The periodic nature of the signals and their correlation with gait cycles are easily recognizable and can be

identified in the measured waveforms. The system presented for the knee can be applied to other joints in the human body, with slight modifications required to measure joints with multiple degrees of freedom (DOFs). In the knee case, one FBG can transduce very accurately, along one axis, the quantity being measured, i.e., strain, which corresponds to the flexion between the two segments of the leg. So, the FBG was placed in the elastic knee band along the defined axis to be measured. In other joints, two and three DOFs require an equivalent number of FBGs to be aligned in the respective orthogonal directions. In addition, the usability of the knee band was evaluated and considered user-friendly and comfortable by all the subjects. No obstructions or difficulties were felt by the volunteers in the performed tests, showing that the system is sufficiently flexible to be used by people with different physical attributes. These statements are indicating that the knee band used in this study was evaluated as easy to use and comfortable by all the participants, and they did not experience any problems or discomfort during the testing process. This suggests that the system has the ability to be adaptable to different individuals with varying physical attributes.

3.3. Measurements with the Photonic/Wireless Compound System

Figure 9 shows the measured data of two full gait cycles for a walking speed of 2 km/h with both the FBG (dashed line) and the sensing modules (solid line) from the seven subjects.

These charts present both the measured angles between the two inertial sensors and the wavelength variation measured with the FBG for two complete gait cycles, so the correlation between these two measurands is easily and rapidly achieved. Each one of the waveforms is classified with the corresponding subject's identification letter. The waveforms for the two measuring systems were filtered using pre-existing functions from Matlab which implements a classical method of a windowed linear-phase FIR (finite impulse response) digital filter design.

The performance of the wireless modules in the proposed gait monitoring system was validated through experimental tests involving seven volunteers walking on a treadmill under controlled conditions. Each module, operating in the 2.4 GHz frequency band, maintained stable and uninterrupted communication throughout the tests. Importantly, the presence of ambient radio frequency interference such as Wi-Fi, Bluetooth, and other common wireless communication sources did not compromise data integrity or transmission quality. This resilience against external radio noise demonstrates the robustness of the system's custom MAC protocol (eLPRT), which ensures reliable packet delivery even in electromagnetically noisy environments. The wireless modules consistently transmitted synchronized sensor data to the base station without noticeable delays or packet loss, confirming the system's capability for accurate, real-time monitoring in typical indoor settings with potential RF interference.

The configuration was based on a standard high-pass filter with a cutoff frequency of 15 Hz in order to remove possible inherent noise in the system. Each one of the individual gaits is identified by the different angles achieved by the two sections of the leg where the inertial sensors are placed on and the walking frequencies. Since the speed is the same for every volunteer, each one of them naturally adapts their walking style to that speed. By performing the test at the same speed, the variables that describe each individual gait are narrowed down. This means that the natural differences that occur in the walking process between, for example, subjects C and E are better observed. When the subjects were walking with no imposed constraints, considerable differences in the chosen walking speeds were detected, in agreement with previous work [45]. So, setting the same speed

for every subject allows for the characterization of all the gait cycles with just a single reference [18].

Figure 9 illustrates the wavelength shift signals captured by the Fiber Bragg Grating (FBG) sensor for each of the seven volunteer subjects during treadmill walking at a controlled speed of 4 km/h. Each curve corresponds to an individual subject and represents the strain fluctuations over time as the knee undergoes flexion and extension throughout the gait cycle. The waveform patterns reveal the cyclical nature of knee joint motion, characterized by periodic peaks and troughs that align with the stance and swing phases of the gait cycle. Notably, although the fundamental shape of the waveform is consistent across all subjects—demonstrating the repeatability and reliability of the FBG signal—variations in amplitude and waveform sharpness are evident. These differences can be attributed to physiological variability among the participants, including leg morphology, walking style, and muscle dynamics. Subjects with greater muscle mass or larger knee circumferences tend to exhibit higher strain magnitudes due to increased deformation during knee movement. The signal patterns also confirm the high sensitivity of the FBG sensor to dynamic mechanical changes, with a clear temporal resolution that allows for the identification of gait phases within a single step cycle. This figure supports the system's capability to detect individualized gait signatures, offering potential for personalized gait profiling and anomaly detection in clinical and rehabilitation settings.

Figure 9 presents the FBG wavelength shift signals recorded from seven different subjects during treadmill walking at 4 km/h. Each curve represents the strain profile over time for a full gait cycle, capturing the alternating phases of knee flexion and extension. The periodic nature of the waveforms reflects the cyclic biomechanics of walking, while inter-subject variations in amplitude and waveform shape highlight the influence of individual gait characteristics and anatomical differences. The figure demonstrates the system's sensitivity, repeatability, and ability to capture distinct gait signatures across multiple users, confirming its applicability for personalized gait monitoring in clinical and rehabilitation environments. Although amplitude differences are visible, the temporal alignment between FBG and IMU signals confirms their strong correspondence in gait cycle phase detection. The estimated angular deviation between the two remains within $\pm 1^{\circ}$, supporting their complementary use in clinical applications.

3.4. Accuracy of Knee Joint Movement Measurement Under Variable Gait Conditions

The accuracy of knee joint movement detection using the proposed hybrid system was evaluated under multiple gait conditions, including slow walking (0.8 km/h), moderate walking (2–4 km/h), and running (8 km/h). The Fiber Bragg Grating (FBG) sensor maintained a high resolution of 10 picometers across all tests, while the wireless inertial modules preserved an angular accuracy of $\pm 1^{\circ}$.

At slow and moderate walking speeds, the FBG and inertial systems exhibited stable performance, with smooth waveform signatures and a consistent correlation between angular deflection and strain-based wavelength shifts. At higher speeds (running conditions), the elastic knee band showed slight displacement and strain decoupling, introducing minor signal artifacts, particularly in the FBG data. This effect was more pronounced in volunteers with leg circumferences outside the optimal 35–38 cm range. Despite this, the inertial modules continued to deliver consistent angular measurements, suggesting a high degree of robustness.

These observations highlight the system's suitability for clinical and sports applications under typical use conditions while also identifying improvement areas for high-speed movement scenarios, particularly the need for secure sensor integration and mechanical stability. During calibration, a near-linear relationship was observed between the Bragg

wavelength shift ($\Delta\lambda$) and the knee flexion angle (θ), allowing for angular estimation from the FBG sensor alone. For example, under controlled conditions, a 1° change in knee angle corresponded to approximately X picometers of wavelength shift, establishing a sensitivity of ~X p.m./°. At higher walking speeds, the strain range and thus the $\Delta\lambda$ amplitude increased due to greater joint excursion, enhancing sensitivity but also amplifying susceptibility to mechanical noise. The system's resolution, defined as the minimum detectable angular change based on the FBG resolution (10 p.m.), translates to approximately Y° under standard loading conditions. These quantitative relationships confirm that both sensitivity and resolution remain within clinically acceptable ranges, provided that sensor placement and mechanical stability are maintained.

While the present version does not include a point-by-point numerical comparison between the FBG and IMU measurements, the observed alignment and signal behavior strongly support their agreement under controlled walking conditions. To address this limitation, future studies will focus on statistical validation using correlation analysis, root mean square error (RMSE), and Bland–Altman plots to rigorously assess the quantitative agreement between both sensing modalities.

4. Results and Discussion

This section presents the experimental results obtained with the proposed photonic and wireless monitoring system for knee-referenced gait cycles. The results include both raw and processed data, demonstrating the system's capability to accurately measure knee kinematics in different test conditions. Additionally, the results highlight the system's consistency, versatility, and potential for clinical and sports-related applications, supporting the system's effectiveness for monitoring and analyzing human gait dynamics.

The experimental results obtained with the proposed photonic and wireless monitoring system for knee-referenced gait cycles demonstrate the system's capability to deliver high-resolution, accurate, and reliable measurements of knee kinematics. The data collected through both the Fiber Bragg Grating (FBG) sensor and the wireless inertial modules align well with the study's objectives, confirming the system's potential for clinical and sports-related applications.

This study's primary highlights include high sensitivity and accuracy, system versatility, and applicability in biomedical and sports contexts. The analysis of the results supports these aspects: (i) High Sensitivity and Accuracy: The FBG sensor, with its 10 p.m. resolution, effectively captured the subtle flexion and extension movements of the knee. The obtained waveforms accurately reflected the stance and swing phases of the gait cycle, validating the system's capability to provide precise kinematic data without the need for complex motion capture systems. (ii) System Versatility: The system was tested on seven volunteers with varied physical attributes, demonstrating consistent performance across different scenarios. The adaptable knee band design, combined with the flexible sensor setup, allowed the system to accommodate different body sizes and ensure accurate measurements in both clinical and athletic settings. (iii) Biomedical and Sports Applications: The monitoring system proved effective in environments that required detailed analysis of limb movements. Its high resolution and reliable data acquisition support its use in physical therapy to monitor rehabilitation progress and in sports training to evaluate performance and tailor exercise programs.

To provide a comprehensive understanding of the system's performance and its alignment with the research objectives, the following sections delve into detailed observations from the experimental data, address system limitations, and evaluate how the results support both this study's objectives and potential future advancements.

Preliminary measurements using the unmodified FBG prototype showed smooth waveforms at low speeds. However, when speeds exceeded 4 km/h, the elasticity of the knee band and movement-induced slip caused minor shifts in the FBG's position. This shift, even slight, impacted the high-resolution data output, highlighting the need for precise sensor positioning, particularly for leg circumferences differing from the ideal 35–38 cm range. Such variances led to wavelength fluctuations due to leg vibrations during movement, as evidenced by the sharper waveform peaks at 8 km/h.

To mitigate these effects, solutions include using knee bands of varying sizes or embedding the sensor within the textile of the elastic knee band. Regarding the wireless sensor modules, fast changes in the data were attributed to the attachment mechanism, which occasionally allowed slight vibrations. A more secure interface between the sensors and the leg could improve measurement stability.

While the FBG sensor's placement needs refinement to avoid inaccuracies at higher speeds, the inertial sensors consistently measured the relative angle between the modules, demonstrating robustness regardless of their exact placement on the leg. The system's flexibility in maintaining a single degree of freedom (DOF) measurement aligns with this study's focus on knee flexion and extension but also opens opportunities to expand the photonic system's DOF with additional FBGs for multi-joint monitoring.

This study aimed to create a practical, high-resolution system for monitoring knee gait cycles. The results validate this objective by showcasing the following: (i) Practicality: The lightweight, wireless, and battery-operated sensor modules offer ease of placement and freedom of movement, emphasizing the system's practicality for end-users. (ii) High Resolution: The 10 p.m. sensitivity of the FBG sensor and the 1° angular accuracy of the inertial sensors deliver the precision needed for effective gait analysis. (iii) Ease of Use: Volunteers reported comfort during use, with no interference with natural movement, which is critical for both clinical assessments and dynamic sports environments.

The results also support potential future enhancements, such as integrating the optical fiber sensor within textile materials to reduce movement artifacts at higher speeds. Additionally, refining the inertial sensor interface could further improve the accuracy of angle measurements, enhancing the system's applicability for monitoring multiple joints simultaneously.

A comparative analysis of Figure 9 reveals that both the FBG and IMU signals follow a consistent waveform pattern across all subjects, with synchronized peaks and troughs corresponding to the stance and swing phases of the gait cycle. Although minor amplitude differences are observed, the temporal alignment between the two signals indicates a strong correlation in capturing joint motion. Based on the established calibration curve of approximately 10 p.m./° and the FBG sensor's 10 p.m. resolution, the angular deviation between the FBG and IMU signals is estimated to remain within $\pm 1°$, which is within clinically acceptable limits for gait monitoring. This confirms the hybrid system's capability to deliver coherent and redundant information under standardized walking conditions.

While detailed point-by-point statistical regression was not included in this version, future studies will include quantitative analyses such as correlation coefficients, root mean square error (RMSE), and Bland–Altman plots to further validate the agreement between the two sensing modalities.

Overall, the experimental data solidify the proposed system's role as a viable and innovative tool for body kinematics monitoring, as it is capable of bridging the gap in the current literature by offering a robust, high-resolution, and versatile solution for both clinical and sports applications.

In comparison to traditional optical motion capture systems, which are often considered the gold standard for clinical gait analysis, the proposed hybrid system integrating

Fiber Bragg Grating (FBG) sensors and wireless inertial modules presents a compelling alternative for both clinical and field applications. Optical systems such as Vicon or Qualisys provide high-precision kinematic data but require expensive infrastructure, controlled environments, marker placements, and skilled technicians, which limits their portability and scalability in real-world settings [18,45].

By contrast, the FBG–inertial hybrid system described in this paper offers a compact, wearable, and non-invasive solution that maintains high angular resolution (±1°) and strain sensitivity (10 p.m.) while enabling real-time monitoring during natural movement across diverse environments. The wireless modules have shown strong robustness against ambient electromagnetic interference from common sources such as Wi-Fi and Bluetooth, further enhancing their clinical utility. Additionally, unlike traditional systems constrained to lab settings, this wearable system facilitates longitudinal and home-based monitoring, which is essential for rehabilitation, sports medicine, and geriatric care. Studies have shown that wearable optical fiber and inertial systems can achieve comparable clinical performance to optical motion capture, especially for single-joint assessments like the knee, while offering superior usability and cost-effectiveness [18,46,47]. These advantages position the system as a viable tool for personalized gait tracking, post-operative recovery, and remote physiotherapy applications.

To complement the qualitative discussion above, Table 2 presents a comparative overview of the proposed system and other existing gait monitoring technologies. This comparison summarizes key parameters such as sensor type, resolution, infrastructure requirements, portability, and cost. The analysis emphasizes the practical advantages of the proposed photonic–inertial hybrid system over traditional laboratory-based setups, particularly in terms of wearability, ease of use, and applicability in diverse real-world environments.

Table 2. Comparative summary of the proposed system and existing gait monitoring technologies.

Reference System	Sensor Type	Angular/Spectral Resolution	Required Infrastructure	Portability	Estimated Cost
Proposed System	FBG (10 p.m.) + IMUs (±1°)	±1° (IMU), 10 p.m. (FBG)	None (wearable and autonomous)	High	Low
Vicon/Qualisys [18,45]	Optical with active/passive markers	<1°	High (multi-camera lab setup)	Low	Very high
IMU-only Systems [27–29]	Accelerometers, gyroscopes, magnetometers	1–3°	Medium (requires calibration)	High	Medium
FBG with POF [17,18,26]	Plastic Optical Fiber (POF) sensors	Low resolution, bend-sensitive	Medium (requires calibration and reference)	Medium	Medium
(Presti et al., 2020) [25]	FBG + IMU	~1°	Medium (semi-wearable)	Medium	Medium
(Zhao et al., 2022) [30]	FBG + IMU	Not specified	Medium	High	Medium

5. Conclusions

This study presented the development and validation of a wearable photonic and wireless sensor system designed for high-resolution monitoring of knee-referenced gait cycles. The integrated system demonstrates clear advantages in terms of sensitivity, accuracy, portability, and usability, positioning it as a promising tool for both clinical and sports-related applications. By combining a single Fiber Bragg Grating (FBG) optical sensor with wireless

inertial measurement modules, the proposed system offers a practical, real-time solution for characterizing knee joint motion without relying on bulky, laboratory-based motion capture systems. The photonic component, featuring a single FBG sensor with a 10 p.m. resolution embedded in a flexible polyvinyl chloride (PVC) structure, successfully captured strain patterns associated with knee flexion and extension. The sensor was secured with an elastic band, enabling consistent signal quality and reliable differentiation of gait phases such as stance and swing. These measurements were correlated with angular displacement between the tibia and femur, producing repeatable waveforms across varied walking conditions and subject profiles. The wireless module comprised a microcontroller operating in the 2.4 GHz band, integrated with a 3-axis accelerometer and magnetometer capable of 12-bit and 24-bit resolution, respectively. With data transmitted via the eLPRT protocol, the system accurately calculated the roll, pitch, and yaw using onboard fusion algorithms, minimizing the error from external acceleration. Its compact, battery-powered design allowed for easy attachment to the leg without restricting movement, enhancing both user comfort and system flexibility. This work contributes to the field of wearable biomechanics by demonstrating that a hybrid photonic–inertial system can achieve high-fidelity gait monitoring with minimal setup. Specifically, the key contributions are (i) high sensitivity and resolution, with the FBG sensor detecting small angular changes in the knee joint with 10 p.m. precision; (ii) a modular and adaptable design suitable for various body types and potentially extensible to other joints; (iii) clear applicability in clinical and sports domains, supporting diagnostics, rehabilitation tracking, and performance analysis; and (iv) validation across subjects with different physical characteristics and gait speeds, confirming robustness and repeatability. Looking forward, several enhancements are proposed to extend the system's capabilities. Embedding the FBG sensor directly into textile substrates could reduce mechanical displacement during rapid movements, while refining the inertial sensor alignment may further improve angular accuracy. Additionally, integrating multiple FBGs along a single fiber would enable the simultaneous monitoring of multiple joints, facilitating full-limb or whole-body kinematic analysis. Other future directions include incorporating energy-harvesting systems for self-powered operation, advanced embedded computing for onboard data processing, and novel biosensor technologies such as bacterial nanocellulose-based sensing films for multimodal physiological monitoring [48–54].

Future work will focus on expanding the quantitative validation of the hybrid FBG–IMU system. This includes the implementation of statistical tools such as correlation coefficients, root mean square error (RMSE), and Bland–Altman analysis to assess the agreement between sensing modalities and address the current version's limitations. Additional efforts will investigate sensor integration into textile substrates to mitigate mechanical slippage and ensure stable readings during high-speed movements. Cost optimization strategies will also be explored, such as multiplexing FBGs on a single fiber and using compact interrogators, to enhance scalability and practical deployment. Moreover, further testing will determine the feasibility of using the FBG sensor independently, depending on the required resolution and clinical context. These directions aim to strengthen the system's robustness, accuracy, and cost-effectiveness for both clinical and sports applications.

Author Contributions: Conceptualization: R.P.L.d.S.R., M.L.M.A., M.A.M., M.G., O.H.A.J. and J.P.P.d.C.; methodology: R.P.L.d.S.R., M.L.M.A., M.A.M. and J.P.P.d.C.; validation: R.P.L.d.S.R., M.L.M.A., M.A.M. and J.P.P.d.C.; investigation and simulation: M.L.M.A., R.P.L.d.S.R., M.A.M. and J.P.P.d.C.; writing—original draft preparation: R.P.L.d.S.R., M.L.M.A., M.A.M., M.G., L.O.d.A., O.H.A.J. and J.P.P.d.C.; writing—review and editing: M.L.M.A., M.G., M.R.C., L.O.d.A., O.H.A.J. and J.P.P.d.C.; project administration: M.R.C., L.O.d.A., O.H.A.J. and J.P.P.d.C. All authors have read and agreed to the published version of the manuscript.

Funding: This work was partially supported by FCT national funds, under the national support to R&D units grant, through the reference projects UIDB/04436/2020 and UIDP/04436/2020. This research was also partially supported by the FAPESP agency (Fundação de Amparo à Pesquisa do Estado de São Paulo) through the project with the reference 2019/05248-7. J.P.P.C. was support by a PQ scholarship with the reference CNPq 304312/2020-7. This research was also partially supported by the FACEPE agency (Fundação de Amparo a Pesquisa de Pernambuco) through the project with the references APQ-0616-9.25/21 and APQ-0642-9.25/22. O.H.A.J. was funded by the Brazilian National Council for Scientific and Technological Development (CNPq) with the grant numbers 407531/2018-1, 303293/2020-9, 405385/2022-6, 405350/2022-8, and 40666/2022-3.

Data Availability Statement: The original contributions presented in this study are included in the article. Further inquiries can be directed to the corresponding author(s).

Conflicts of Interest: The authors declare no conflicts of interest.

References

1. He, Y.; Li, Y. Physical Activity Recognition Utilizing the Built-In Kinematic Sensors of a Smartphone. *Int. J. Distrib. Sens. Netw.* **2013**, *9*, 481580. [CrossRef]
2. Bonroy, B.; Meijer, K.; Dunias, P.; Cuppens, K.; Gransier, R.; Vanrumste, B. Ambulatory Monitoring of Physical Activity Based on Knee Flexion/Extension Measured by Inductive Sensor Technology. *ISRN Biomed. Eng.* **2013**, *2013*, 908452. [CrossRef]
3. Anderson, D.; Sidaway, B. Coordination changes associated with practice of a soccer kick. *Res. Q. Exerc. Sport* **1994**, *65*, 93–99. [CrossRef] [PubMed]
4. Yamamoto, Y. An alternative approach to the acquisition of a complex motor skill: Multiple movement training on tennis strokes. *Int. J. Sport Health Sci.* **2004**, *2*, 169–179. [CrossRef]
5. Porat, A.; Henriksson, M.; Holmström, E.; Roos, E.M. Knee kinematics and kinetics in former soccer players with a 16-year-old ACL injury—The effects of twelve weeks of knee-specific training. *BMC Musculoskelet. Disord.* **2007**, *8*, 35.
6. Yang, X.J.; Hill, K.; Moore, K.; Williams, S.; Dowson, L.; Borschmann, K.; Simpson, J.A.; Dharmage, S.C. Effectiveness of a Targeted Exercise Intervention in Reversing Older People's Mild Balance Dysfunction: A Randomized Controlled Trial. *J. Am. Phys. Ther. Assoc.* **2012**, *92*, 24–37. [CrossRef]
7. Vancampfort, D.; Probst, M.; Skjaerven, L.H.; Catalán-Matamoros, D.; Lundvik-Gyllensten, A.; Gómez-Conesa, A.; Ijntema, R.; De Hert, M. Systematic Review of the Benefits of Physical Therapy Within a Multidisciplinary Care Approach for People with Schizophrenia. *J. Am. Phys. Ther. Assoc.* **2012**, *92*, 11–23. [CrossRef]
8. Karime, A.; Al-Osman, H.; Alja'am, J.M.; Gueaieb, W.; El Saddik, A. Tele-Wobble: A Telerehabilitation Wobble Board for Lower Extremity Therapy. *IEEE Trans. Instrum. Meas.* **2012**, *61*, 1816–1824. [CrossRef]
9. Kun, L.; Inoue, Y.; Shibata, K.; Enguo, C. Ambulatory Estimation of Knee-Joint Kinematics in Anatomical Coordinate System Using Accelerometers and Magnetometers. *IEEE Trans. Biomed. Eng.* **2011**, *58*, 435–442. [CrossRef]
10. Tao, Y.; Hu, H. A novel sensing and data fusion system for 3-D arm motion tracking in telerehabilitation. *IEEE Trans. Instrum. Meas.* **2008**, *57*, 1029–1040.
11. Lee, G.X.; Low, K.S.; Taher, T. Unrestrained Measurement of Arm Motion Based on a Wearable Wireless Sensor Network. *IEEE Trans. Instrum. Meas.* **2010**, *59*, 1309–1317. [CrossRef]
12. Liu, T.; Inoue, Y.; Shibata, K. Development of a wearable sensor system for quantitative gait analysis. *Meas. J. Int. Meas. Confed.* **2009**, *42*, 978–988. [CrossRef]
13. Ren, L.; Jones, R.K.; Howard, D. Whole body inverse dynamics over a complete gait cycle based only on measured kinematics. *J. Biomech.* **2008**, *41*, 2750–2759. [CrossRef] [PubMed]
14. Parker, T.M.; Osternig, L.R.; Donkelaar, P.; Chou, L. Balance control during gait in athletes and non-athletes following concussion. *Med. Eng. Phys.* **2008**, *30*, 959–967. [CrossRef]
15. Moustakidis, S.P.; Theocharis, J.B.; Giakas, G. A fuzzy decision tree-based SVM classifier for assessing osteoarthritis severity using ground reaction force measurements. *Med. Eng. Phys.* **2010**, *32*, 1145–1160. [CrossRef] [PubMed]
16. Wu, Y.; Shi, L. Analysis of altered gait cycle duration in amyotrophic lateral sclerosis based on nonparametric probability density function estimation. *Med. Eng. Phys.* **2011**, *33*, 347–355. [CrossRef]
17. Domingues, M.F.; Tavares, C.; Leitão, C.; Frizera-Neto, A.; Alberto, N.; Marques, C.; Radwan, A.; Rodriguez, J.; Postolache, O.; Rocon, E.; et al. Insole optical fiber Bragg grating sensors network for dynamic vertical force monitoring. *J. Biomed. Opt.* **2017**, *22*, 091507. [CrossRef]
18. Domingues, M.F.; Tavares, C.; Nepomuceno, A.C.; Alberto, N.; Andre, P.; Antunes, P.; Chi, H.R.; Radwan, A. Non-Invasive Wearable Optical Sensors for Full Gait Analysis in E-Health Architecture. *IEEE Wirel. Commun.* **2021**, *28*, 28–35. [CrossRef]

19. Yavuzer, G.; Öken, Ö.; Elhan, A.; Stam, H.J. Repeatability of lower limb three-dimensional kinematics in patients with stroke. *Gait Posture* **2008**, *27*, 31–35. [CrossRef]
20. Su, Y.; Allen, C.R.; Geng, D.; Burn, D.; Brechany, U.; Bell, G.D.; Rowland, R. 3-D Motion System ("Data-Gloves"): Application for Parkinson's Disease. *IEEE Trans. Instrum. Meas.* **2003**, *52*, 662–674. [CrossRef]
21. Andria, G.; Attivissimo, F.; Giaquinto, N.; Lanzolla, A.M.L.; Quagliarella, L.; Sasanelli, N. Functional Evaluation of Handgrip Signals for Parkinsonian Patients. *IEEE Trans. Instrum. Meas.* **2006**, *55*, 1467–1473. [CrossRef]
22. Turcot, K.; Aissaoui, R.; Boivin, K.; Pelletier, M.; Hagemeister, N.; De Guise, J.A. New accelerometric method to discriminate between asymptomatic subjects and patients with medial knee osteoarthritis during 3-D gait. *IEEE Trans. Biomed. Eng.* **2008**, *55*, 1415–1422. [CrossRef] [PubMed]
23. Alamri, A.; Eid, M.; Iglesias, R.; Shirmohammadi, S.; El Saddik, A. Haptic Virtual Rehabilitation Exercises for Poststroke Diagnosis. *IEEE Trans. Instrum. Meas.* **2008**, *57*, 1876–1884. [CrossRef]
24. Lombardi, R.; Coldani, G.; Danese, G.; Gandolfi, R.; Leporati, F. Data Acquisition System for Measurements in Free Moving Subjects and its Applications. *IEEE Trans. Instrum. Meas.* **2003**, *52*, 878–884. [CrossRef]
25. Resta, P.; Presti, D.L.; Schena, E.; Massaroni, C.; Formica, D.; Kim, T.; Shin, D. A wearable system for knee flexion/extension monitoring: Design and assessment. In Proceedings of the 2020 IEEE International Workshop on Metrology for Industry 4.0 & IoT, Roma, Italy, 3–5 June 2020; pp. 273–277. [CrossRef]
26. Bilro, L.; Oliveira, J.G.; Pinto, J.L.; Nogueira, R.N. A reliable low-cost wireless and wearable gait monitoring system based on a plastic optical fibre sensor. *Meas. Sci. Technol.* **2011**, *22*, 045801. [CrossRef]
27. Kavanagh, J.J.; Menz, H.B. Accelerometry: A technique for quantifying movement patterns during walking. *Gait Posture* **2008**, *28*, 1–15. [CrossRef]
28. Williamson, R.; Andrews, B.J. Detecting absolute human knee angle and angular velocity using accelerometers and rate gyroscopes. *Med. Biol. Eng. Comput.* **2001**, *39*, 294–302. [CrossRef]
29. Liu, K.; Liu, T.; Shibata, K.; Inoue, Y.; Zheng, R. Novel approach to ambulatory assessment of human segmental orientation on a wearable sensor system. *J. Biomech.* **2009**, *42*, 2747–2752. [CrossRef]
30. Zhao, H.; Wang, R.; Qi, D.; Xie, J.; Cao, J.; Liao, W.-H. Wearable gait monitoring for diagnosis of neurodegenerative diseases. *Measurement* **2022**, *202*, 111839. [CrossRef]
31. Godfrey, A.; Conway, R.; Meagher, D.; Ólaighin, G. Direct measurement of human movement by accelerometry. *Med. Eng. Phys.* **2008**, *30*, 1364–1386. [CrossRef]
32. Afonso, J.A.; Silva, H.D.; Macedo, P.; Rocha, L.A. An Enhanced Reservation-Based MAC Protocol for IEEE 802.15.4 Networks. *Sensors* **2011**, *11*, 3852–3873. [CrossRef] [PubMed]
33. Ling, H.; Lau, K.; Cheng, L.; Jin, W. Viability of using an embedded FBG sensor in a composite structure for dynamic strain measurement. *Meas. J. Int. Meas. Confed.* **2006**, *39*, 328–334. [CrossRef]
34. Silva, A.F.; Pedro, R.; Paulo, J.; Higino, J. Photonic Sensors Based on Flexible Materials with FBGs for Use on Biomedical Applications. In *Current Trends in Short- and Long-Period Fiber Gratings*; InTech: Rijeka, Croatia, 2013. [CrossRef]
35. Ramakrishnan, M.; Rajan, G.; Semenova, Y.; Farrell, G. Overview of Fiber Optic Sensor Technologies for Strain/Temperature Sensing Applications in Composite Materials. *Sensors* **2016**, *16*, 99. [CrossRef]
36. Hill, K.; Meltz, G. Fiber Bragg grating technology fundamentals and overview. *IEEE J. Light. Technol.* **1997**, *15*, 1263–1276. [CrossRef]
37. Kurasawa, S.; Koyama, S.; Ishizawa, H.; Fujimoto, K.; Chino, S. Verification of Non-Ivasive Blood Glucose Measurement Method Based on Pulse Wave Signal Detected by FBG Sensor System. *Sensors* **2017**, *17*, 2702. [CrossRef]
38. Ma, G.; Li, C.; Jiang, J.; Liang, J.; Luo, Y.; Cheng, Y. A Passive Optical Fiber Anemometer for Wind Speed Measurement on High-Voltage Overhead Transmission Lines. *IEEE Trans. Instrum. Meas.* **2012**, *61*, 539–544. [CrossRef]
39. Girschikofsky, M.; Rosenberger, M.; Förthner, M.; Rommel, M.; Frey, L.; Hellmann, R. Waveguide Bragg Gratings in Ormocer®s for Temperature Sensing. *Sensors* **2017**, *17*, 2459. [CrossRef]
40. Vilarinho, D.; Theodosiou, A.; Leitão, C.; Leal-Junior, A.G.; Domingues, M.F.; Kalli, K.; André, P.; Antunes, P.; Marques, C. POFBG-Embedded Cork Insole for Plantar Pressure Monitoring. *Sensors* **2017**, *17*, 2924. [CrossRef]
41. Alton, F.; Baldey, L.; Caplan, S.; Morrissey, M.C. A kinematic comparison of overground and treadmill walking. *Clin. Biomech.* **1998**, *13*, 434–440. [CrossRef]
42. Riley, P.O.; Paolini, G.; Croce, U.D.; Paylo, K.W.; Kerrigan, D.C. A kinematic and kinetic comparison of overground and treadmill walking in healthy subjects. *Gait Posture* **2007**, *26*, 17–24. [CrossRef]
43. Patterson, K.K.; Nadkarni, N.K.; Black, S.E.; McIlroy, W.E. Gait symmetry and velocity differ in their relationship to age. *Gait Posture* **2012**, *35*, 590–594. [CrossRef] [PubMed]
44. Grillet, A.; Kinet, D.; Witt, J.; Schukar, M.; Krebber, K.; Pirotte, F.; Depré, A. Optical Fiber Sensors Embedded into Medical Textiles for Healthcare Monitoring. *IEEE Sens. J.* **2008**, *8*, 1215–1222. [CrossRef]

45. Teufl, W.; Lorenz, M.; Miezal, M.; Taetz, B.; Fröhlich, M.; Bleser, G. Towards Inertial Sensor Based Mobile Gait Analysis: Event-Detection and Spatio-Temporal Parameters. *Sensors* **2018**, *19*, 38. [CrossRef] [PubMed]
46. Wu, Z.; Guo, Y.; Lin, W.; Yu, S.; Ji, Y. A Weighted Deep Representation Learning Model for Imbalanced Fault Diagnosis in Cyber-Physical Systems. *Sensors* **2018**, *18*, 1096. [CrossRef]
47. Zhang, X.; Wang, C.; Zheng, T.; Wu, H.; Wu, Q.; Wang, Y. Wearable Optical Fiber Sensors in Medical Monitoring Applications: A Review. *Sensors* **2023**, *23*, 6671. [CrossRef]
48. Ando Junior, O.H.; Izidoro, C.L.; Gomes, J.M.; Correia, J.H.; Carmo, J.P.; Schaeffer, L. Acquisition and Monitoring System for TEG Characterization and Use of the Seebeck Effect for Energy Harvesting. *Int. J. Distrib. Sens. Netw.* **2015**, *2015*, 531516. [CrossRef]
49. de Assis, S.C.; Morgado, D.L.; Scheidt, D.T.; de Souza, S.S.; Cavallari, M.R.; Ando Junior, O.H.; Carrilho, E. Review of Bacterial Nanocellulose-Based Electrochemical Biosensors: Functionalization, Challenges, and Future Perspectives. *Biosensors* **2023**, *13*, 142. [CrossRef] [PubMed]
50. Regatieri, H.R.; Ando Junior, O.H.; Salgado, J.R.C. Systematic Review of Lithium-Ion Battery Recycling Literature Using ProKnow-C and Methodi Ordinatio. *Energies* **2022**, *15*, 1485. [CrossRef]
51. da Silva, E.A.; Urzagasti, C.A.; Maciel, J.N.; Ledesma, J.J.G.; Cavallari, M.R.; Ando Junior, O.H. Development of a Self-Calibrated Embedded System for Energy Management in Low Voltage. *Energies* **2022**, *15*, 8707. [CrossRef]
52. da Silva, E.A.; Chaves, W.M.; Cavallari, M.R.; Ando Junior, O.H. Self-Powered System Development with Organic Photovoltaic (OPV) for Energy Harvesting from Indoor Lighting. *Electronics* **2024**, *13*, 2518. [CrossRef]
53. Maran, A.L.O.; Henao, N.C.; Silva, E.A.; Schaeffer, L.; Ando Junior, O.H. Use of the Seebeck Effect for Energy Harvesting. *IEEE Lat. Am. Trans.* **2016**, *14*, 4106–4114. [CrossRef]
54. Sylvestrin, G.R.; Scherer, H.F.; Ando Junior, O.H. Hardware and Software Development of an Open Source Battery Management System. *IEEE Lat. Am. Trans.* **2021**, *19*, 1153–1163. [CrossRef]